



OPEN Effect of ice cover roughness on local scour around bridge piers

Shihao Dong¹, Zhenhua Zhang¹, Jun Wang^{1✉} & Jueyi Sui²

In cold-region rivers, the formation of ice cover during winter markedly modifies the hydraulic conditions, leading to enhanced local scour around in-stream infrastructures such as bridge piers. To analyze the flow characteristics and maximum local scour depth around the pier under both open-channel and ice-covered conditions with varying roughness, both experimental methods and numerical simulations were employed in this study. The findings reveal that, under rough ice-covered flow conditions, the interaction of elevated bed shear stress and intensified turbulent kinetic energy contributes to an increased maximum scour depth around the pier. Under identical approaching flow conditions, when the ratio of ice cover roughness to bed roughness increases to 1.9, the increase in maximum local scour depth around the pier becomes less pronounced owing to the enhanced energy dissipation caused by the rough ice cover. A numerical model for local scour around the pier under open-channel flow and ice-covered flow conditions was developed by integrating the RNG $k-\epsilon$ turbulence model with the Meyer-Peter sediment transport equation. A new formula was developed to estimate the maximum local scour depth around bridge piers considering various ice cover roughness conditions. Comparison with existing formulas demonstrates that the proposed formula achieves the highest accuracy, offering a useful reference for the design of bridge foundations in ice-affected regions.

Keywords Ice cover roughness, Bridge pier, Local scour, Maximum scour depth, Turbulent kinetic energy, Numerical simulation

Abbreviations

B	Flume width
B/D	Flume width to pier diameter ratio
D	Pier diameter
d_{50}	Median particle diameter
d_s	Maximum local scour depth
Fr	Froude number
G	Gravitational acceleration
H	Approaching flow depth
k_s	Roughness coefficient
κ	Von Kármán constant
n_i	Manning roughness coefficient of the ice cover
n_b	Manning roughness coefficient of the riverbed
n_i/n_b	Ratio of ice cover roughness to riverbed roughness
ρ_s	Sand mass density
Q	Flow rate
TKE	Turbulent kinetic energy
u^*	Shear velocity
U	Approaching flow velocity
U_a	Average velocity
U_c	Incipient sediment motion in open channel flow
U/U_c	Flow intensity
y	Distance of the bottom ice cover surface
Z	Distance from the riverbed

¹School of Civil and Hydraulic Engineering, Hefei University of Technology, Hefei 230009, China. ²School of Engineering, University of Northern British Columbia, 3333 University Way, Prince George BC V2N 4Z9, Canada. ✉email: junwanghfut@126.com

Ice covers are widely distributed in rivers located in high-latitude cold regions of the Southern and Northern Hemispheres^{1,2}. The presence of ice cover alters the vertical distribution of flow velocity in rivers, intensifies the turbulent kinetic energy near the channel bed, and significantly increases bed shear stress^{3,4}. These changes in hydraulic characteristics often exacerbate local scour around the in-stream infrastructures such as bridge piers. Globally, the intensification of local scour around bridge piers is one of the primary causes of instability of bridges⁵. Consequently, accurate prediction of the maximum scour depth around bridge piers under ice-covered flow conditions is essential for ensuring the structural safety of bridges in cold regions.

To date, researchers have typically employed experimental and numerical simulation approaches to study the local scour process around bridge piers, with most studies focusing on scour around piers in straight flumes under open-channel flow conditions^{6–10}. However, the presence of ice covers in rivers alters factors such as channel roughness and flow velocity distribution, influencing sediment transport and rendering the problem of local scour around bridge piers more complex¹¹. Zabilansky and White¹² investigated the impact of ice cover on local scour in narrow channels through experimental and field studies, revealing that the presence of a fixed ice cover increases hydrostatic pressure, shifts the maximum flow velocity toward the riverbed, and intensifies local scour around the pier. Wang et al.¹³ conducted experimental research and found that the threshold velocity for sediment initiation under ice-covered flow conditions is markedly lower than under open flow conditions. As ice cover roughness increases, the threshold velocity for sediment initiation decreases. Wu et al.¹⁴ investigated local scour around semi-circular abutments by varying ice cover roughness. They observed a 35% increase in maximum scour depth under rough ice covers compared with that under smooth ice covers. Wu et al.¹⁵ performed experimental studies on local scour around bridge piers and observed that, when varying water depth, the presence of an ice cover markedly influences the maximum local scour depth at shallow flow conditions. As the Froude number of the pier increases, the maximum local scour depth decreases. Empirical formulas were developed to estimate the scour depth and scour radius around the pier under both open-channel and ice-covered flow conditions. Valela et al.¹⁶ conducted experimental studies on local scour around the pier under ice-covered flow conditions by varying the submergence depth of the ice cover. Their results demonstrated that as the submergence depth increased, the flow Froude number rose, leading to an increase in the maximum local scour depth around the pier. Sirianni et al.¹⁷ experimentally investigated the influence of upstream ice cover length on the maximum local scour depth. Their findings revealed that the maximum scour depth did not monotonically increase with ice cover length. It peaked when the upstream ice cover length reached 2.66 m (half of the maximum tested length), after which further increases in ice cover length resulted in reduced maximum scour depth and scour hole volume. Wang et al.¹⁸ performed pier scour experiments under open and ice-covered flow conditions, systematically varying flow parameters, median sediment size, and pier diameter. Their results indicated that the maximum local scour depth under ice-covered flows was approximately 20–30% greater than under open flow conditions, while the scour range and volume increased by 40–50%. Based on these data, they proposed empirical formulas to predict the maximum scour depth and scour hole volume. Through experimental investigations, Gao et al.¹⁹ demonstrated that during local scour around bridge piers under ice-covered flow conditions, sediment particle motion is primarily dominated by jet and sweep flow patterns. Through multi-factor orthogonal experiments, they optimized the geometric shape of anti-scour plates, reducing the maximum local scour depth around bridge piers, with better protective effects observed under rough ice-covered flow conditions.

During the experimental process, constraints such as equipment limitations and cost considerations made it challenging to comprehensively account for all factors influencing bridge pier scour, while also restricting in-depth investigation of complex flow field structures²⁰. Given these limitations inherent to experimental research, numerical simulation has emerged as a critical method for studying local scour around bridge piers²¹. Vasquez and Walsh²² employed the RNG $k-\epsilon$ turbulence model to replicate flow characteristics such as horseshoe vortices and downflow around the pier. They compared their simulation results with experimental data from Melville²³ and achieved good agreement. Khosronejad et al.²⁴ investigated local scour around the pier of different shapes using both experimental and numerical simulations methods. They found that the URANS equations were unable to accurately simulate horseshoe vortices, and the scour simulation results for the leading edges of circular and square pier were relatively poor. In contrast, diamond-shaped pier generated smaller horseshoe vortices, allowing for better simulation of their local scour. Zhao et al.²⁵ conducted numerical simulations using the $k-\omega$ SST turbulence model to study the effects of varying pier height-to-diameter ratios (h_p/D) on local scour. Their research indicated that scour depth decreased as h_p/D decreased. For $h_p/D \geq 2$, pier height had a minimal impact on scour depth, and the scour depth tended to stabilize; in contrast, for $h_p/D < 2$, scour depth was significantly influenced by pier height. Kalidindi et al.²⁶ employed the LES turbulence model to study the evolution of scour holes around circular piers, revealing the dynamic characteristics of horseshoe vortex systems during intermediate stages and their impact on bed shear stress. Hamidi et al.²⁷ adopted a combined numerical simulation and experimental validation approach to investigate the effects of varying configurations of dual vanes, including height, length, installation angle, position angle, and the distance of the dual vanes from the pier on reducing maximum local scour depth. Their study found that when vanes are attached to piers at a 90° installation angle, the maximum local scour depth can be reduced by approximately 33%, yielding the most significant effect. However, when vane height exceeds the sediment deposit height (2D), the trend of maximum scour depth reduction diminishes. Al-Jubouri et al.²⁸ utilized the RNG $k-\epsilon$ turbulence model for numerical simulations and experiments to examine the influence of pier geometry and debris accumulation on scour. Their results indicated that square piers exhibit the greatest scour depth, while lenticular piers show the least. An increase in the debris-to-pier diameter ratio significantly alters vortex structures in the flow field, leading to scour depth differences of up to 5 cm. Hamidi et al.²⁹ employed numerical simulations and experimental validation to study scour characteristics around piers of different shapes when mining pits exist downstream. Their findings revealed that higher pit heights and closer proximity to piers exacerbate scour severity, with

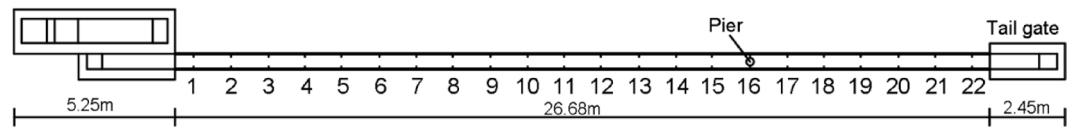


Fig. 1. The layout of the experiment facility.

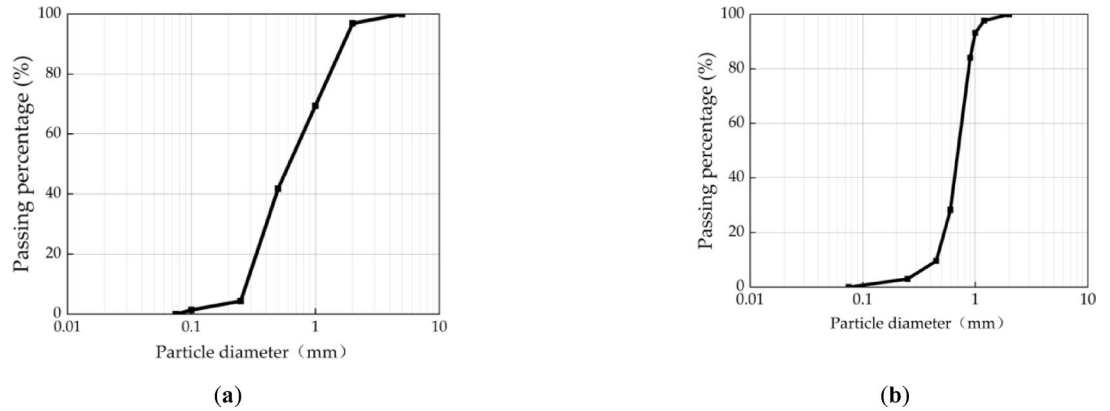


Fig. 2. Grain size distribution curves: (a) $d_{50} = 0.44$ mm; (b) $d_{50} = 0.71$ mm.

circular piers experiencing the greatest scour depth and airfoil piers the least. Gupta et al.³⁰ conducted LES-based numerical simulations to investigate the effects of Air-Foil Collars with varying diameters and installation heights on local pier scour. Their results demonstrated that such collars could reduce maximum scour depth by 11% to 100%, with good agreement between simulated and experimental data.

Numerical simulation studies on pier scour under ice-covered flow conditions remain limited³¹. Namaee et al.³² employed the RNG k- ϵ turbulence model for numerical simulations to investigate local scour around the semi-circular and rectangular abutments under open, smooth ice-covered, and rough ice-cover flow conditions. Their results indicated that the maximum local scour depth for rectangular abutments occurred at the upstream right-angle corner, while for semi-circular abutments, it was located at a 75° angle to the flow direction. Compared to open flow conditions, the presence of an ice cover increased the maximum local scour depth around the abutment, with the rough ice-covered flow condition exhibiting the largest increases in turbulent kinetic energy and maximum local scour depth. In addition to abutment studies, Namaee et al.³³ also conducted numerical simulations using the RNG k- ϵ model to study local scour around double piers in side-by-side arrangements under open, smooth ice-covered, and rough ice-covered flow conditions. Their findings indicated that as the median sediment grain size increased, the maximum local scour depth around the pier decreased. Additionally, as the roughness of the ice cover increased, the location of the maximum flow velocity shifted closer to the riverbed. Gao et al.³⁴ used the RNG k- ϵ turbulence model to simulate flow field characteristics around tandem double piers under open and ice-covered flow conditions. Their results showed that ice covers primarily affect the flow field around piers by increasing drag in the upper-middle water layers, leading to redistribution of flow structures. Additionally, ice covers elevate turbulent kinetic energy and bed shear stress.

In summary, the formation of ice covers in rivers within cold winter regions significantly alters the flow structure around bridge piers. As a critical factor influencing the interaction between river flow and piers, variations in ice cover roughness directly affect the local scouring process and equilibrium scour depth of bridge piers. Current research on ice-induced pier scour during freezing periods has primarily focused on two types of ice cover roughness, smooth and rough, while lacking systematic analysis of continuous roughness variations characteristic of naturally occurring ice covers. This study quantifies, through numerical simulation and experimental methods, the variation patterns of the maximum velocity point location within the flow velocity distribution when ice cover roughness changes, along with its impacts on bed shear stress, turbulent kinetic energy, and maximum local scour depth. The findings provide a reference for bridge construction in cold-region rivers and help mitigate the risk of bridge instability during ice periods.

Methods

Experimental model

Experiments were conducted in a flume measuring 26.68 m in length, 0.4 m in width, and 1.3 m in depth, as shown in Fig. 1. From cross section 1 to cross section 22, a 10 cm-thick layer of sand was placed in the flume bed. Given the non-uniform sediment composition in natural rivers, non-uniform sediments were used to simulate the natural riverbed. The median sediment grain sizes (d_{50}) were 0.71 mm and 0.44 mm, with corresponding standard deviations (σ) of 1.61 and 1.85. The mass density of sediment was 2610 kg/m³. The sediment grain size distribution curves are presented in Fig. 2. The critical velocity of sediment deposits (U_c) was calculated

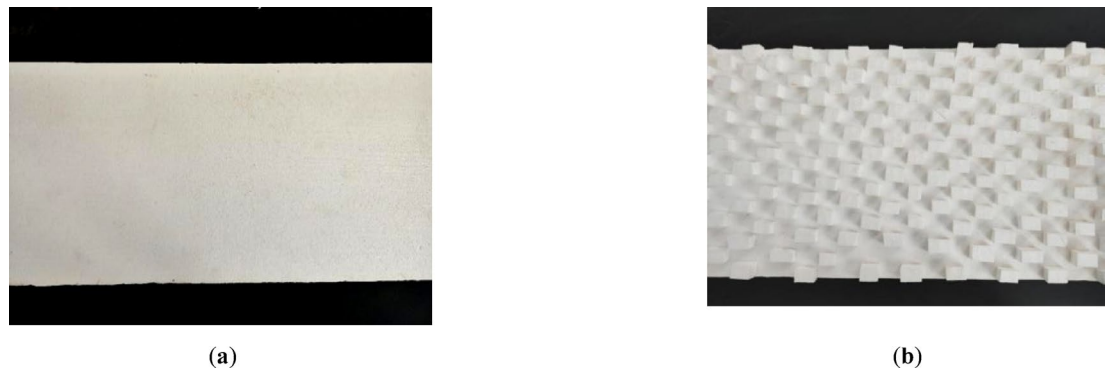


Fig. 3. Simulation of (a) smooth ice cover and (b) rough ice cover.



Fig. 4. Experimental Site Photograph: (a) flume; (b) pier scour.

using the formula proposed by Melville and Sutherland³⁵. The pier was fixed at the center of cross section 16, as depicted in Fig. 1. Cylindrical pier with diameters of 3 cm and 4 cm were used in this study. The minimum ratio of flume width to pier diameter (B/D) in this experiment was 10. Lança et al.³⁶ concluded through flume experiments that sidewall effects can be neglected when $B/D > 5$. Therefore, sidewall effects were considered negligible in this study.

The smooth ice cover was fabricated using Styrofoam panels, while the rough ice cover was created by adhering small Styrofoam cubes to the bottom of the smooth ice cover. Each Styrofoam cube measured 30 mm \times 30 mm \times 30 mm, with a spacing of 30 mm between adjacent cubes (Fig. 3). The simulated ice cover materials used in this experiment are commonly employed in ice hydraulics research^{37–39}. The experimental site photograph is presented in Fig. 4.

Under ice-covered flow conditions, varying ice cover roughness significantly influences flow structure⁴⁰, thereby inducing complex effects on the local scour process around the pier. The ice cover roughness (k_s) can be determined using Eq. (1) by fitting the velocity distribution near the ice cover (from the water surface to the position of maximum flow velocity) based on the logarithmic wall law¹⁷. Here, U_a represents the average velocity at a distance y of the bottom ice cover surface, u^* is the shear velocity, and κ is the von Kármán constant ($\kappa = 0.41$).

$$U_a = \left(\frac{u^*}{\kappa} \right) \ln y + \left(\frac{u^*}{\kappa} \right) \ln \left(\frac{30}{k_s} \right) \quad (1)$$

$$n_i = 0.039k_s^{\frac{1}{6}} \quad (2)$$

Figure 5 presents the regression results for the velocity profile extending from the water surface to the point of maximum flow velocity under ice-covered flow conditions. By performing regression fitting on the velocity profile that adheres to the logarithmic wall law, the calculated slope and intercept were substituted into Eq. (1) to determine the k_s for smooth and rough ice covers as 0.0307 m and 0.0056 m, respectively. Substituting k_s into Eq. (2)⁴¹, the Manning coefficients for smooth and rough ice covers were calculated as 0.016 and 0.022, respectively. Barahimi and Sui⁴² compared different methods for calculating ice cover Manning roughness coefficients and found that this approach yielded relatively small errors. Carey et al.⁴³ measured velocity distributions in rivers under real ice-covered flow conditions and calculated ice cover Manning coefficients ranging from 0.01 to 0.0281, with winter ice covers typically having a Manning coefficient of 0.0251, which is

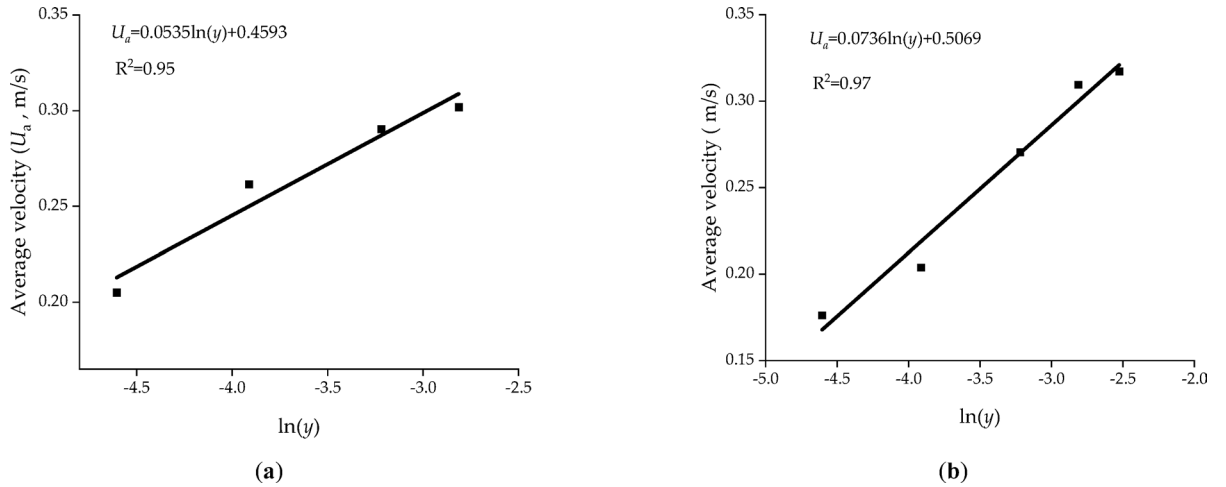


Fig. 5. Linear regression using the wall approximation law: **(a)** smooth ice cover; **(b)** rough ice cover.

relatively close to the value obtained for rough ice covers in this experiment. The bed Manning coefficient (n_b) was calculated using Eq. (3)⁴⁴. The experiment employed a propeller-type current meter to measure flow velocity distribution, with a relative measurement error of 5%.

$$n_b = 0.039d_{50}^{\frac{1}{6}} \tag{3}$$

Prior to the experiment, water was gradually introduced into the flume to prevent bed scour. The weir head corresponding to the experimental flow rate was calculated using the weir flow formula, and the pump valve was adjusted to match the calculated weir head, ensuring the flume achieved the desired flow rate. The tailgate was adjusted to maintain the flow velocity and flow depth at the specified experimental conditions. The simulated ice cover was then carefully placed on the water surface, and the pier was inserted into the channel bed at cross section 16. Compared to open flow conditions, the presence of ice covers significantly prolongs the time required for bridge pier scour to reach equilibrium, with experimental durations lasting 10–12 hours. This study adopts the equilibrium scour criterion proposed by Mia and Nago⁴⁵, defining equilibrium as achieved when the scour depth variation rate falls below 1 mm/h. Once the scour depth around pier reached its maximum value, the flume was slowly drained. To accurately measure scour depths at various locations and plot the scour hole contour map, the area around the pier was uniformly divided and marked. The measurement error for the maximum scour depth was ± 0.1 mm. In this study, a total of 29 experimental runs were conducted, with specific experiment conditions detailed in Table 1.

Numerical model

The study employed Flow-3D V11.2 software for simulations. Flow-3D utilizes the Volume of Fluid (VOF) method to track water surfaces. Hirt et al.⁴⁶ proposed the Fractional Area/Volume Obstacle Representation (FAVOR) technique to simulate complex geometric shapes⁴⁷. Compared to the Finite Difference Method (FDM), the FAVOR approach enables geometric resolution with fewer computational grids, thereby reducing calculation time⁴⁸.

Governing equations

The governing equations for incompressible Newtonian fluids, comprising the Reynolds-Averaged Navier-Stokes (RANS) equations and the continuity equation, are expressed by Eqs. (4–7).

$$\frac{\partial}{\partial x_i} (u_i A_i) = 0 \tag{4}$$

$$\frac{\partial u}{\partial t} + \frac{1}{V_F} \left(u_i A_i \frac{\partial u_i}{\partial x_j} \right) = -\frac{1}{\rho} \frac{\partial P}{\partial x_i} + g + f_i \tag{5}$$

$$\rho V_F f_i = \tau_{b,i} - \left[\frac{\partial P}{\partial x_j} (A_i S_{ij}) \right] \tag{6}$$

$$S_{ij} = -(\mu + \mu_T) \left(\frac{\partial u_i}{\partial x_j} + \frac{\partial u_j}{\partial x_i} \right) \tag{7}$$

Here, u_i denotes the velocity component in the i -direction, V_F represents the fluid volume fraction within each computational cell, and A_i indicates the fractional area open to flow in the i -direction. P is the pressure, ρ is the

Number	Ice cover roughness (n_i)	Approaching flow velocity (U , m/s)	Approaching flow depth (H , m)	Flow Froude number (Fr)	Pier diameter (D , cm)	Median grain sizes (d_{50} , mm)
1	Open flow	0.18	0.15	0.148	4	0.71
2		0.22	0.15	0.181	4	0.71
3		0.22	0.20	0.157	4	0.71
4		0.22	0.10	0.222	4	0.71
5		0.26	0.15	0.214	4	0.71
6		0.18	0.15	0.148	3	0.71
7		0.22	0.15	0.181	3	0.71
8		0.26	0.15	0.214	3	0.71
9		0.18	0.15	0.148	3	0.44
10		0.22	0.15	0.181	3	0.44
11		0.26	0.15	0.214	3	0.44
12	Smooth ice-covered flow	0.18	0.15	0.148	4	0.71
13		0.22	0.15	0.181	4	0.71
14		0.22	0.20	0.157	4	0.71
15		0.22	0.10	0.222	4	0.71
16		0.26	0.10	0.263	2	0.71
17		0.26	0.15	0.214	4	0.71
18		0.18	0.15	0.148	3	0.71
19		0.22	0.15	0.181	3	0.71
20		0.26	0.15	0.214	3	0.71
21		0.18	0.15	0.148	3	0.44
22		0.22	0.15	0.181	3	0.44
23	0.26	0.15	0.214	3	0.44	
24	Rough ice-covered flow	0.18	0.15	0.148	4	0.71
25		0.22	0.15	0.181	4	0.71
26		0.26	0.15	0.214	4	0.71
27		0.18	0.15	0.148	3	0.71
28		0.22	0.15	0.181	3	0.71
29		0.26	0.15	0.214	3	0.71

Table 1. Experimental conditions summary.

Turbulence model	d_s/H			RMSE	MAE
	Number 1	Number 2	Number 5		
k- ϵ	0.163	0.131	0.111	0.0204	0.018
RNG k- ϵ	0.281	0.235	0.249	0.0181	0.013
LES	0.327	0.322	0.303	0.0182	0.018

Table 2. Comparison of statistical errors between experimental and simulated maximum local scour depths around bridge piers.

fluid mass density, and t is time, g corresponds to the gravitational acceleration, f_i is the diffusion transport term, and S_{ij} is the strain rate tensor. The wall shear stress is denoted as $\tau_{b,i}$, and the total dynamic viscosity combines both molecular viscosity (μ) and eddy viscosity (μ_T).

Turbulent model

In the FLOW-3D numerical model, turbulence in hydraulic problems is commonly simulated using the k- ϵ , RNG k- ϵ , and LES (Large Eddy Simulation) models⁴⁹. By comparing the simulated maximum local scour depths around bridge piers obtained from these three turbulence models with experimental data (as shown in Table 2), we can observe that the RNG k- ϵ and LES models yield smaller errors in predicting the maximum scour depth. However, compared to the LES model, which requires fine meshing for accurate simulation, the RNG k- ϵ model significantly reduces computational time⁵⁰. Considering both error margins and computational efficiency, the RNG k- ϵ turbulence model was selected for this study. Its governing equations include area and volume fractions, similar to the inclusion approach in the continuity and momentum conservation equations^{51,52}.

$$\frac{\partial k}{\partial t} + \frac{\partial}{\partial x_i} (ku_i) = \frac{\partial}{\partial x_j} \left[\left(\mu + \frac{\mu}{\sigma_k} \right) \frac{\partial k}{\partial x_j} \right] + P_k - \varepsilon \quad (8)$$

$$\frac{\partial \varepsilon}{\partial t} + \frac{\partial}{\partial x_i} (\varepsilon u_i) = \frac{\partial}{\partial x_j} \left[\left(\mu + \frac{\mu}{\sigma_\varepsilon} \right) \frac{\partial \varepsilon}{\partial x_j} \right] + C_{1\varepsilon} \frac{\varepsilon}{k} P_k - C_{2\varepsilon}^* \rho \frac{\varepsilon^2}{k} \quad (9)$$

where:

$$P_k = \nu_T SS \quad (10)$$

$$S = \sqrt{\frac{1}{2} \left(\frac{\partial u_j}{\partial x_i} + \frac{\partial u_i}{\partial x_j} \right)^2} \quad (11)$$

The constant values for the turbulence model are $C_{1\varepsilon}=1.42$, $C_{2\varepsilon}^*=1.68$, and $\sigma_k = \sigma_\varepsilon = 0.7194$ ⁵².

Sediment transport model

The accelerated flow around the pier induces significant shear stress on the adjacent sediment. When bed shear stress exceeds the critical shear stress, sediment entrainment occurs. Sediment particles begin to move when the local Shields parameter (θ_i) surpasses the critical Shields number ($\theta_{cr,i}$). These phenomena are defined by the following equations:

$$\theta_i = \frac{\tau}{\|g\| d_i (\rho_i - \rho_f)} \quad (12)$$

where: τ_b is the bed shear stress; d_i is the median grain size of sediment type i ; ρ_i is the density of sediment type i ; ρ_f is the fluid density. $\theta_{cr,i}$ can be calculated using the Soulsby⁵³ equation:

$$\theta_{cr,i} = \frac{0.3}{1 + 1.2d_*} + 0.055 [1 - \exp(-0.02d_*)] \quad (13)$$

d_* is the dimensionless grain diameter of sediment, which can be calculated using the following equation:

$$d_* = d_i \left[\frac{(\rho_i - \rho_f) \rho_f \|g\|}{\mu_f^2} \right]^{\frac{1}{3}} \quad (14)$$

where: μ_f is the fluid dynamic viscosity.

Sediment deposition refers to the process where sediment particles settle from suspension to the riverbed under gravitational force. According to Mastbergen⁵⁴, the lifting velocity for sediment entrainment can be calculated as follows:

$$u_{lift,i} = \alpha_i n_s d_*^{0.3} (\theta_i - \theta_{cr,i})^{1.5} \sqrt{\frac{\|g\| d_i (\rho_i - \rho_f)}{\rho_f}} \quad (15)$$

The settling velocity of sediment particles is given by Soulsby⁵⁵:

$$u_{setting,i} = \frac{v_f}{d_i} \left[(10.36^2 + 1.049d_*^3)^{0.5} - 10.36 \right] \quad (16)$$

The concentration of suspended sediment is calculated by solving its transport equation:

$$\frac{\partial C_{s,i}}{\partial t} + \nabla \cdot (u_{s,i} C_{s,i}) = \nabla \cdot \nabla (D_f C_{s,i}) \quad (17)$$

where: D_f is the diffusion coefficient; $u_{s,i}$ is the velocity of suspended sediment, and $C_{s,i}$ represents the sediment concentration.

For bed load transport, the sediment transport rate on the riverbed can be calculated using the Meyer-Peter⁵⁶ equation as follows:

$$\phi_i = \beta_i (\theta_i - \theta_{cr,i})^{1.5} \quad (18)$$

where β_i is the bed load coefficient, typically set to 8.0.

The volumetric bed load transport rate $q_{b,i}$ is calculated by:

$$q_{b,i} = \phi_i \left[\|g\| \left(\frac{\rho_i - \rho_f}{\rho_f} \right) d_i^3 \right]^{\frac{1}{2}} \quad (19)$$

Number	Ice cover roughness (n_i)	Approaching velocity (U , m/s)	Approaching depth (H , m)	Flow Froude number (Fr)	Pier diameter (D , cm)	Median grain sizes (d_{50} , mm)
1	0.010	0.18	0.15	0.214	4	0.71
2	0.028	0.18	0.15	0.214	4	0.71
3	0.034	0.18	0.15	0.214	4	0.71
4	0.010	0.22	0.15	0.181	4	0.71
5	0.028	0.22	0.15	0.181	4	0.71
6	0.034	0.22	0.15	0.181	4	0.71
7	0.010	0.26	0.15	0.181	4	0.71
8	0.028	0.26	0.15	0.181	4	0.71
9	0.034	0.26	0.15	0.181	4	0.71

Table 3. Simulation conditions summary.

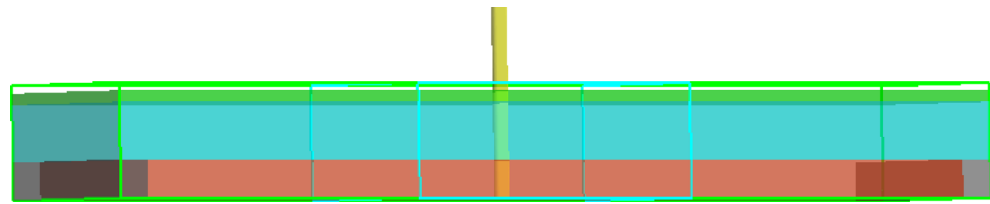


Fig. 6. Boundary condition setup.

The accuracy of numerical simulations for local scour is significantly influenced by the calculation formulas for different $q_{b,i}$. Li et al.⁵⁷ investigated the discrepancies among these three equations. Their results demonstrated that using the Meyer-Peter equation⁵⁶ yields the smallest relative error in predicting the maximum local scour depth around the pier. Therefore, this study adopts the Meyer-Peter⁵⁶ sediment transport equation for calculations, with the bed load coefficient set to 8.

Model setup

A total of 38 numerical simulations of local scour around bridge piers were conducted. To validate the numerical results against experimental data under open, smooth ice-covered, and rough ice-covered flow conditions, 28 simulations were performed with parameters matching those of the experiments (Table 1). Additionally, 9 simulations were carried out to investigate the effects of varying ice cover roughness on flow characteristics and pier scour under ice-covered flow conditions, as detailed in Table 3. To avoid redundant presentation, only the results of these 9 newly added simulations are shown in this study. The critical shear stress was calculated using the equation derived by Soulsby⁵³. According to Mastbergen⁵⁴, the default entrainment coefficient was set to 0.018, while the default angle of repose for sediment was 32°.

The boundary conditions are specifically configured as shown in Fig. 6. The flow moves from left to right, passing around the pier and inducing local scour in its vicinity before exiting the computational domain. For the upstream inlet, a velocity boundary condition is applied; the outlet is set as outflow. The sidewalls are designated as wall boundaries, while the top boundary is treated as a symmetric boundary, and the bottom boundary is also set as a wall boundary. For different ice cover roughness conditions, the experimentally measured ice cover roughness height is specified to match the corresponding ice cover Manning coefficient. Fixed sand beds of equal height and width are laid at both the upstream and downstream sections of the sand bed, with surface roughness consistent with that of the movable sand bed.

In numerical simulations, the size of the computational domain and grid resolution significantly influence the simulation results. A nested grid approach was employed to locally refine the mesh around the pier, maintaining a 2:1 size ratio between coarse and fine grids. The coarse grid covered the entire computational domain, with a 1.5 m long fine grid nested at the center. The length of the computational domain was selected as 6.2 m. According to Sarker's research⁵⁸, the presence of a pier affects flow patterns up to 6D upstream and 12D downstream. Since the upstream and downstream computational domains extend beyond 6D and 12D respectively, the flow can fully develop within the domain. Therefore, the computational domain size is considered reasonable. To determine optimal grid resolution while maintaining the 2:1 coarse-to-fine grid ratio, the influence of grid size variations on the maximum local scour depth around the pier was investigated, as shown in Fig. 7. As the mesh is refined, the maximum local scour depth around the bridge pier gradually stabilizes. Although a slight fluctuation in the rate of change of scour depth occurs when reducing the mesh size from 10 to 9 mm, relative to subsequent finer mesh results, this represents pre-convergent non-monotonic behavior, commonly observed in strongly separated flows due to the high sensitivity of vortex structures to minor geometric or resolution variations⁵⁹. Such phenomena are not necessarily caused by simulation errors. Turbulence models sensitive to mesh resolution are more prone to exhibiting this behavior. Therefore, a 5 mm mesh was adopted in this study,

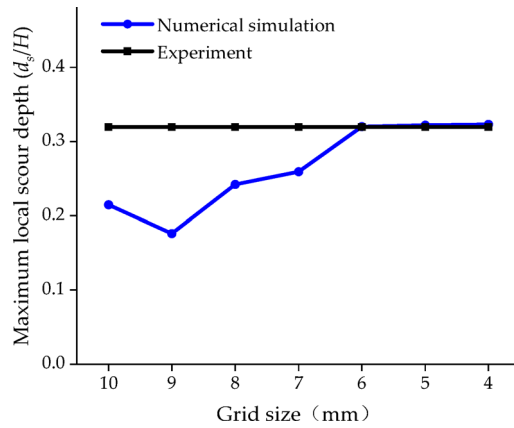


Fig. 7. Grid independence verification.

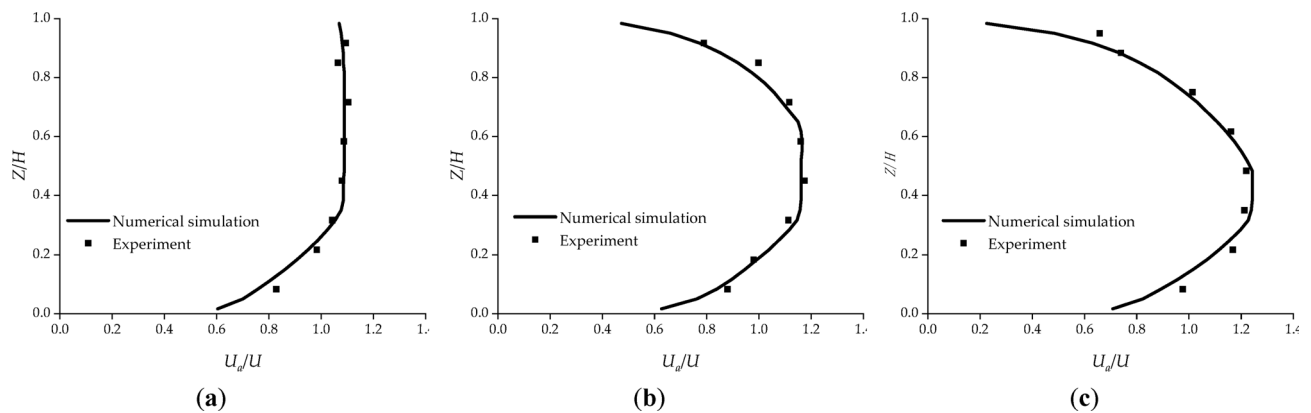


Fig. 8. Vertical velocity distribution profile at the channel center under different flow conditions: (a) open; (b) smooth ice cover; (c) rough ice cover.

balancing minimal discretization error with reasonable computational time. Under these conditions, the fine grid contained 960,000 cells (96w) and the coarse grid contained 384,000 cells (38.4w).

Results

Model validation

Local scour around the pier is primarily influenced by factors such as flow velocity distribution and bed shear stress⁶⁰. Analyzing velocity distributions under different flow conditions is crucial for understanding scour mechanisms around the pier. Figure 7 illustrates the vertical velocity profiles at the centerline of the riverbed under various flow conditions. The figure shows that under open flow conditions, the flow velocity exhibits a logarithmic distribution, with the maximum velocity occurring near the water surface. When an ice cover is present, the velocity distribution transforms into a bilogarithmic velocity profile⁶¹. Compared to smooth ice-covered flow conditions, the position of the maximum velocity point shifts further toward the riverbed under rough ice-covered flow conditions. This occurs because increased ice cover roughness causes the maximum velocity point to migrate toward surfaces with lower flow resistance¹¹. The Manning coefficient under smooth ice-covered flow conditions is $n_i = 0.016$, while under rough ice-covered flow conditions it is $n_i = 0.022$. The riverbed Manning coefficient is $n_b = 0.019$. A comparison was conducted between the numerically simulated and experimentally measured vertical velocity profiles of flow under different flow conditions (Fig. 8). The results demonstrate that the simulated vertical velocity distributions of flow can accurately reflect actual flow characteristics, with a mean absolute percentage error (MAPE) of 4.30%. Therefore, this numerical model is considered reliable for simulating flow velocity distributions under both open and ice-covered flow conditions.

Figure 9 presents the contour maps of riverbed elevation around the pier during the equilibrium scour stage under open, smooth ice-covered, and rough ice-covered flow conditions. As shown in Fig. 9, the simulated maximum local scour depth around the pier occurs at approximately a 45° angle to the flow direction, which is consistent with the simulation results reported by Khosronejad et al.²⁴ and Kim et al.⁶². This is primarily attributed to flow acceleration around the pier, which maximizes shear stress in this region, resulting in the deepest local scour at this location. Compared to open flow conditions, the presence of the smooth ice cover increases the maximum local scour depth, while rough ice-covered flow conditions induce even greater scour

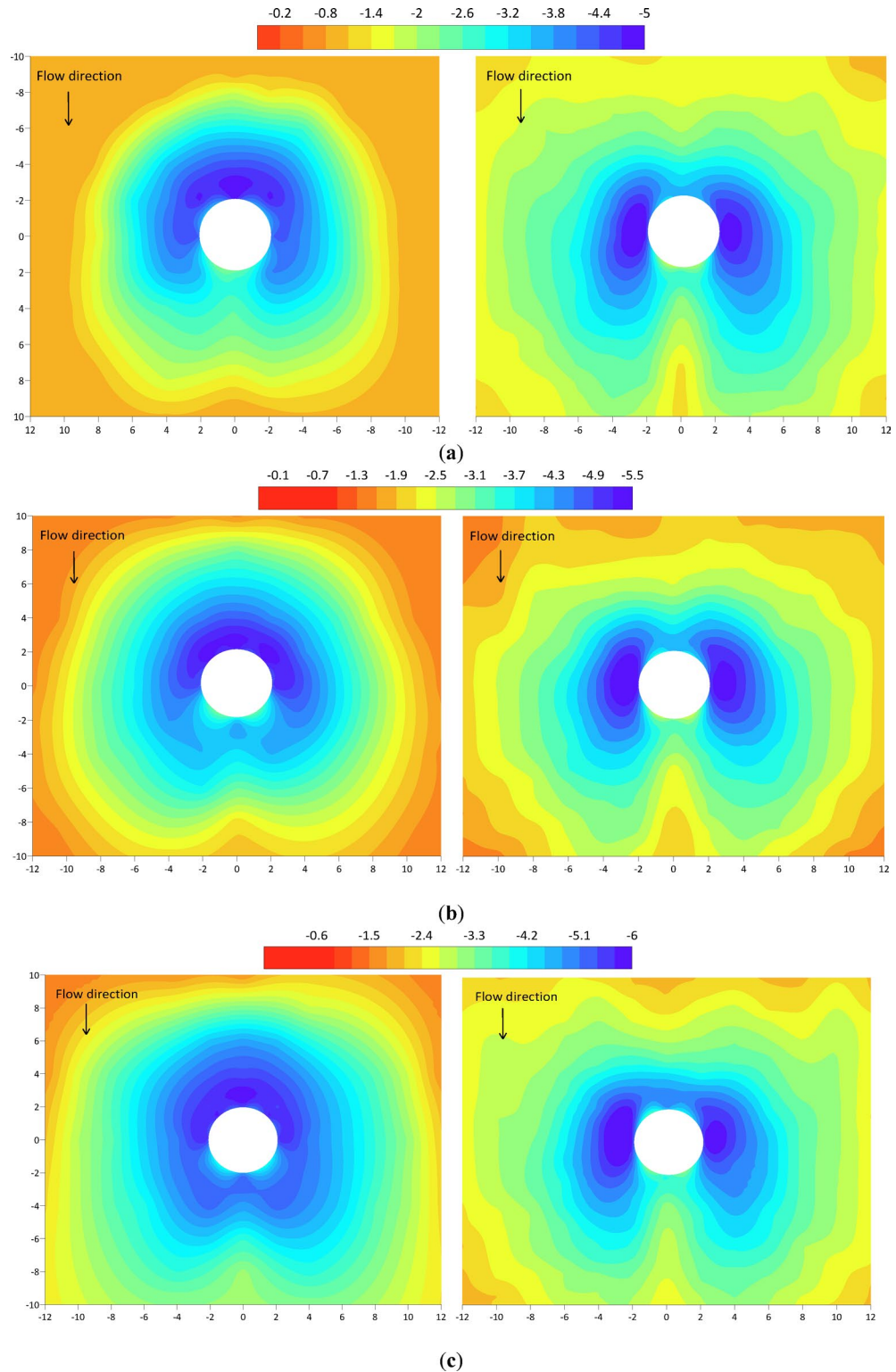


Fig. 9. Contour maps of riverbed elevation around the pier during the equilibrium scour stage under open, smooth ice-covered, and rough ice-covered flow conditions. Left: Experimental results; Right: Simulated results. (a) open; (b) smooth ice cover; (c) rough ice cover.

depths. Figure 10 compares the simulated and experimental values of maximum local scour depth around the pier under open, smooth ice-covered, and rough ice-covered flow conditions, with specific experiment conditions detailed in Table 1. As illustrated in Fig. 10, the MAPE between experimental and simulated values of maximum local scour depth is 10.91% across different flow conditions, indicating good agreement. By comparing both the

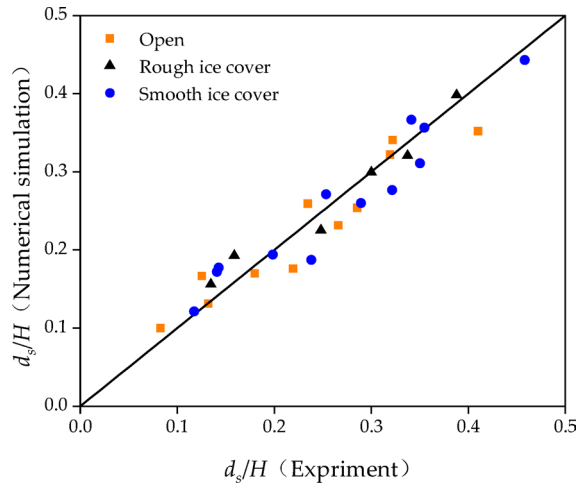


Fig. 10. Relationship between simulated and measured values of maximum local scour depth around the pier.

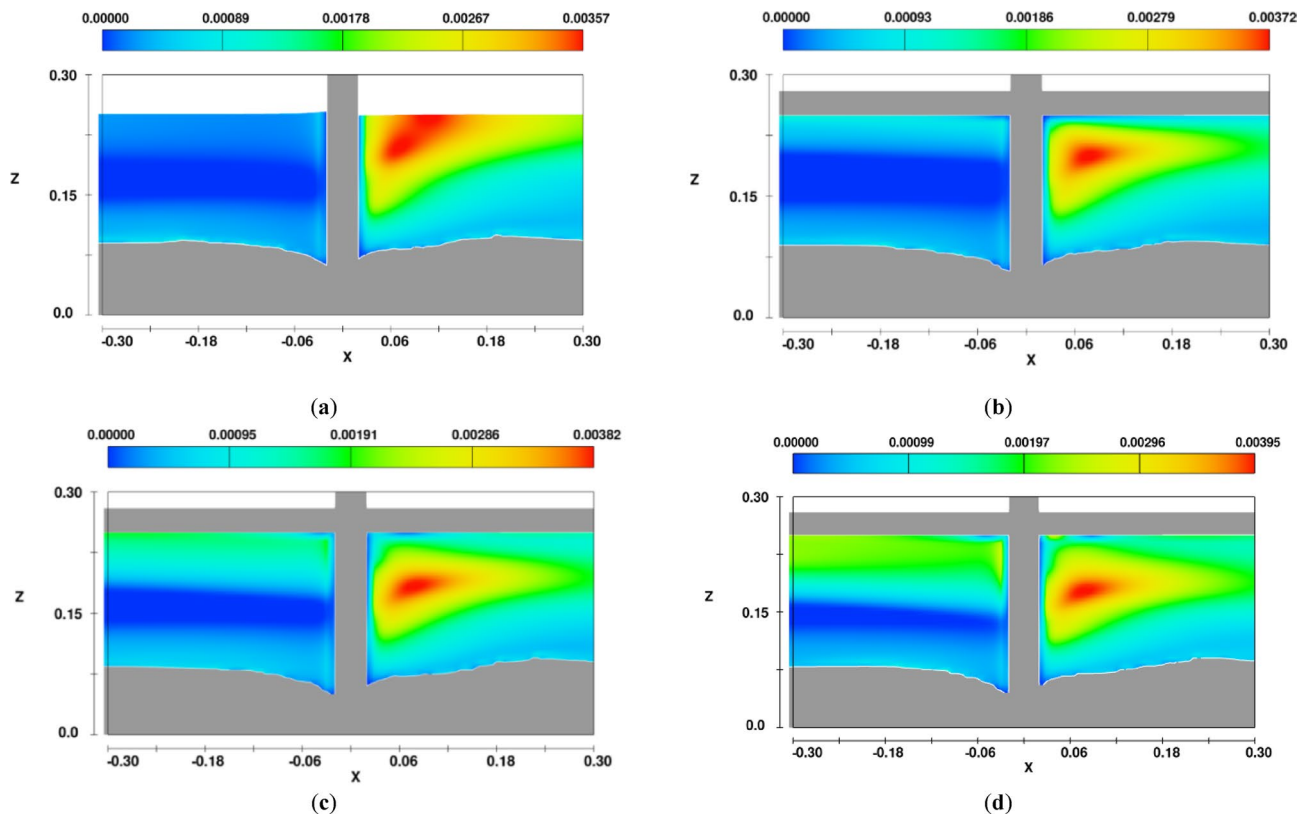


Fig. 11. Simulated distribution of TKE around the pier in the X–Z cross-section during the equilibrium scour stage under different flow conditions: (a) open flow; (b) $n_i/n_b = 1.4$; (c) $n_i/n_b = 1.9$; (d) $n_i/n_b = 2.4$.

maximum scour depths and scour hole morphologies from experiments and simulations, the developed model is considered to effectively simulate local scour around the pier under ice-covered conditions.

Flow characteristics under different ice cover conditions

Figure 11 presents the simulated distribution of turbulent kinetic energy (TKE) around the pier in the X–Z cross-section during the equilibrium scour stage under different flow conditions. Figure 12 shows the vertical distribution of TKE under varying ice cover roughness. The TKE is calculated as $TKE = 0.5 (\overline{u'^2} + \overline{v'^2} + \overline{w'^2})$, where u' , v' , and w' represent the fluctuations of instantaneous velocities from their mean values in the streamwise, transverse, and vertical directions, respectively. TKE quantifies turbulence intensity by calculating the combined

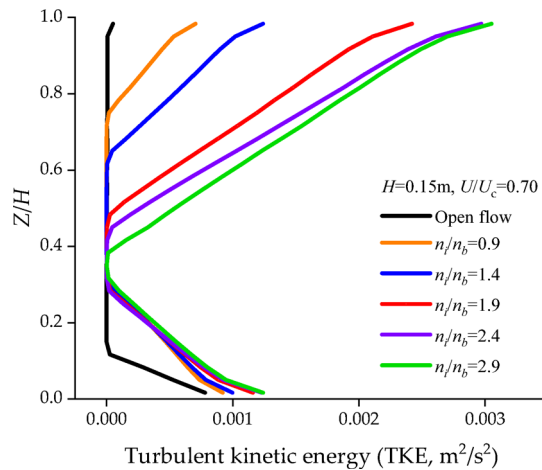


Fig. 12. Simulated vertical distribution of TKE under different ice cover roughness conditions.

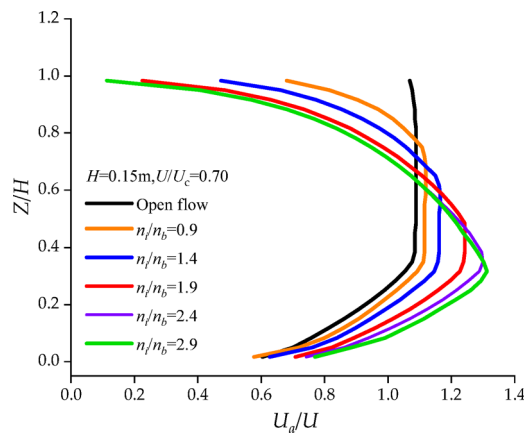


Fig. 13. Simulated vertical velocity profiles at the bed center under varying ice cover roughness conditions.

energy of velocity fluctuations in all three directions. Higher TKE values indicate stronger turbulent phenomena, typically associated with shear layers, flow separation, and vortex formation³⁹. As shown in Figs. 11 and 12, under open flow conditions, TKE values near the water surface upstream of the pier are relatively low. The presence of an ice cover transforms the free water surface into a shear boundary layer, resulting in increased TKE values in this region. With increasing ice cover roughness, TKE near the riverbed ($Z/H < 0.3$) increases by approximately 8% to 35%, while TKE near the ice cover bottom ($Z/H > 0.8$) increases by 76% to 332% relative to the open flow condition. Additionally, the area with near zero TKE values upstream of the pier decreases as ice cover roughness increases, consistent with the simulation results of Namaee et al.³³. Due to the strong wake vortices behind the pier, the maximum TKE values occur downstream of the pier under both open and ice-covered flow conditions. Under open flow, the maximum TKE appears near the water surface downstream of the pier, whereas under ice-covered flow conditions, the maximum TKE shifts toward the riverbed and increases in magnitude with increasing ice cover roughness.

To investigate the effects of varying ice cover roughness on flow characteristics, simulations were conducted to analyze the vertical velocity distribution, migration patterns of the maximum velocity point, and variations in bed shear stress, as shown in Figs. 13, 14 and 15. Figure 13 indicates that as ice cover roughness increases, the flow velocity distribution undergoes significant changes. The region with a gentle velocity gradient ($0.4 < Z/H < 0.8$) noticeably shrinks due to enhanced frictional resistance at the ice-water interface and TKE caused by higher roughness. This alters the vertical velocity profile, resulting in greater non-uniformity in the intermediate flow region, which aligns with Yoon et al.'s⁶⁵ findings on velocity distribution beneath ice covers. Figures 14 and 15 demonstrate that increased ice cover roughness shifts the maximum velocity point from $Z/H = 0.68$ to $Z/H = 0.35$, intensifying the velocity gradient in the near-bed region ($Z/H < 0.4$) and subsequently increasing bed shear stress. Compared to open flow conditions, bed shear stress (τ_b) increases by approximately 7% to 42% under ice-covered flow conditions as roughness increases. The bed shear stress was calculated using the method described in Reference⁶⁴, where $\tau_b = \rho u_*^2$, with u_* representing the shear velocity and ρ representing the fluid density.

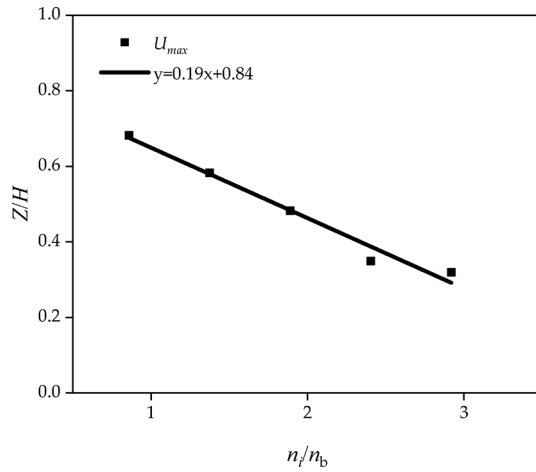


Fig. 14. Location of maximum velocity points under simulated ice cover roughness conditions.

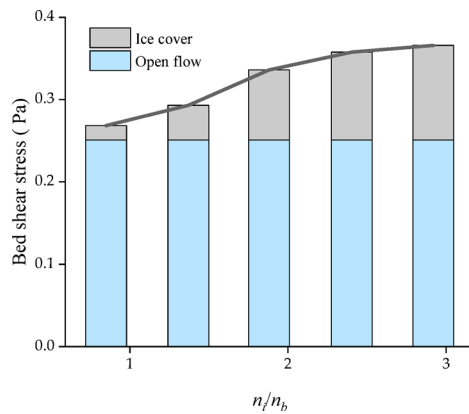


Fig. 15. Variation of bed shear stress under simulated ice cover roughness conditions.

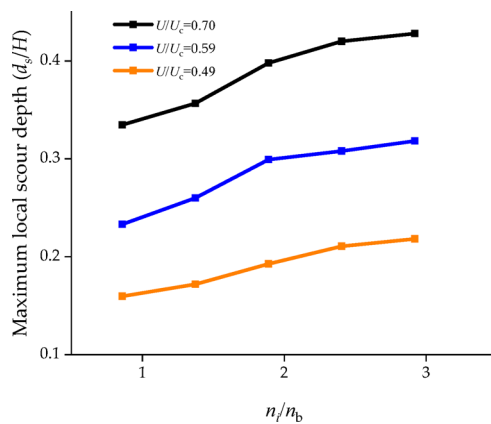


Fig. 16. Variation of maximum local scour depth around the pier under simulated ice cover roughness conditions.

Impact of ice cover roughness on maximum scour depth

By varying ice cover roughness, simulations were conducted to analyze changes in maximum local scour depth around the pier and the temporal evolution of scour depth, as shown in Fig. 16 and 17. Figure 16 indicates that when other conditions remain constant, the maximum local scour depth (d_s/H) increases with the ratio of ice cover roughness to bed roughness (n_i/n_b). However, when $n_i/n_b < 1.9$, d_s/H exhibits a relatively rapid increase

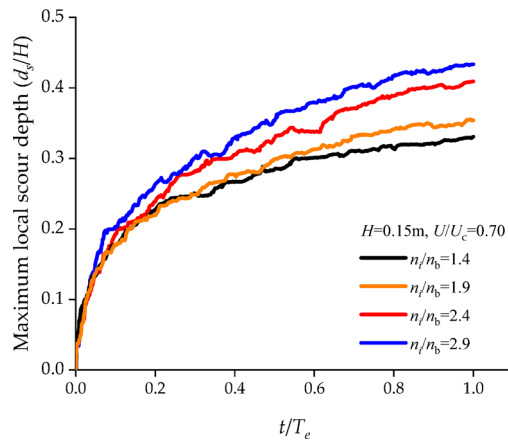


Fig. 17. Variation of maximum local scour depth around the pier over normalized time (t/T_e) under simulated ice cover roughness conditions, where T_e denotes the total simulated time.

with n_i/n_b , whereas the rate of increase slows when $n_i/n_b > 1.9$. This phenomenon can be explained by the preceding text. Additionally, as ice cover roughness increases, TKE generation beneath the ice cover intensifies, leading to greater energy dissipation in the flow. Consequently, the enhancement of TKE and bed shear stress near the riverbed diminishes (as shown in Figs. 12 and 15), resulting in reduced sediment transport capacity at the bed surface and a subsequent attenuation in the rate of increase for maximum local scour depth. Figure 17 demonstrates that under identical conditions, an increase in n_i/n_b not only elevates the local scour depth around the pier but also accelerates the temporal rate of scour depth. This remains attributable to the enhanced sediment transport capacity of near-bed flows caused by increased n_i/n_b .

Equations for predicting the maximum scour depth under ice-covered flow conditions

After comprehensively considering the relevant variables in the experiments, the relationship between the maximum local scour depth under ice-covered flow conditions and the primary variables influencing scour depth is expressed as follows:

$$d_s = f(D, d_{50}, g, H, n_i, n_b, U) \quad (20)$$

In the equation, d_s represents the maximum local scour depth around the bridge pier, D denotes the pier diameter, d_{50} is the median sediment grain size, g is the gravitational acceleration, H is the initial water depth, n_i is the Manning roughness coefficient of the ice cover, n_b is the Manning roughness coefficient of the riverbed, and U is the initial flow velocity—all of which are finite parameters. Based on dimensional analysis, Eq. (20) can be expressed in the following dimensionless form:

$$\frac{d_s}{H} = f\left(\frac{U}{\sqrt{gH}}, \frac{d_{50}}{D}, \frac{n_i}{n_b}\right) \quad (21)$$

Here, d_s/H represents the relative equilibrium scour depth, U/\sqrt{gH} denotes the flow Froude number, d_{50}/D is the ratio of median sediment grain size to pier diameter, and n_i/n_b indicates the ratio of ice cover roughness to riverbed roughness. Equation (21) can be transformed into Eq. (22) as follows:

$$\frac{d_s}{H} = k \left(\frac{U}{\sqrt{gH}}\right)^a \left(\frac{d_{50}}{D}\right)^b \left(\frac{n_i}{n_b}\right)^c \quad (22)$$

In the equation, k , a , b , and c are coefficients.

Based on the experimental and numerical simulation data in this study, Equation (23) was derived through fitting a total of 27 datasets. Among these, 70% (19 datasets) were used for training, while 30% (8 datasets) were allocated for validation. The following regression equation is established

$$\frac{d_s}{H} = 1.14 \left(\frac{U}{\sqrt{gH}}\right)^{2.21} \left(\frac{d_{50}}{D}\right)^{-0.53} \left(\frac{n_i}{n_b}\right)^{0.29} \quad (23)$$

Sensitivity analysis was conducted to evaluate the effective parameters and quantify their impacts on the maximum scour depth around bridge piers beneath ice covers. All effective parameters were incorporated, including flow velocity, water depth, median sediment grain size, pier diameter, ice cover roughness, and riverbed roughness. As shown in Table 4, the flow Froude number demonstrates the most significant influence on scour depth prediction ($R^2 = 0.043$, $RMSE = 0.098$, $MAE = 0.083$), followed by the ratios of ice cover roughness

Model	Equation variables	R ²	RMSE	MAE
1	$\frac{d_s}{H} = f\left(\frac{U}{\sqrt{gH}}, \frac{d_{50}}{D}, \frac{n_i}{n_b}\right)$	0.922	0.030	0.024
2	$\frac{d_s}{H} = f\left(\frac{d_{50}}{D}, \frac{n_i}{n_b}\right)$	0.043	0.098	0.083
3	$\frac{d_s}{H} = f\left(\frac{U}{\sqrt{gH}}, \frac{n_i}{n_b}\right)$	0.856	0.033	0.026
4	$\frac{d_s}{H} = f\left(\frac{U}{\sqrt{gH}}, \frac{d_{50}}{D}\right)$	0.862	0.032	0.025

Table 4. Sensitivity analysis of effective parameters.

Parameter	Domain application							
	Equation (23)		Equation (24)		Equation (25)		Equation (26)	
	Mini	Max	Mini	Max	Mini	Max	Mini	Max
U/\sqrt{gH}	0.148	0.262	0.104	0.196	0.109	0.195	0.157	0.262
d_{50}/D	0.015	0.036	0.011	0.011	0.011	0.011	0.015	0.036
n_i/n_b	0.858	2.919	1.054	1.532	1.532	1.532	1.116	1.209

Table 5. Application scope of the formulas.

to riverbed roughness (n_i/n_b) and median sediment grain size to pier diameter (d_{50}/D), which also affect pier scour under ice-covered conditions.

The formula proposed by Valela et al.¹⁶ for calculating bridge pier scour under smooth ice-covered conditions is as follows:

$$\frac{d_s}{D} = 0.87 \ln\left(\frac{U^2}{gD}\right) + 2.96 \tag{24}$$

The formula proposed by Valela et al.¹⁶ for calculating bridge pier scour under rough ice-covered flow conditions is as follows:

$$\frac{d_s}{D} = 1.22 \ln\left(\frac{U^2}{gD}\right) + 3.89 \tag{25}$$

The formula proposed by Wang et al.¹⁸ for calculating bridge pier scour under ice cover conditions:

$$\frac{d_s}{H} = 1.81 \left(\frac{U - U_c}{\sqrt{gH}}\right)^{0.942} \left(\frac{d_{50}}{H}\right)^{-0.177} \left(\frac{D}{H}\right)^{0.60} \left(\frac{n_i}{n_b}\right)^{0.30} \tag{26}$$

The application scope of the formulas for calculating the maximum local scour depth around bridge piers under ice cover conditions is presented in Table 5.

The data in Fig. 18 are derived from References^{16,18}, as well as all experimental data on bridge pier scour under ice-covered flow conditions collected in this study. All datasets, including those from Valela et al.¹⁶, Wang et al.¹⁸, and our experiments were calculated using Eqs. (23–26). The computational results and error statistics are presented in Fig. 18 and Table 6, respectively. For the determination of n_i/n_b in References^{16,18}, n_i was established based on their simulated materials, while n_b was computed using Eq. (3). Among these, Eq. (23) yielded the smallest calculation errors for maximum local scour depth around bridge piers. This is primarily because, in contrast to the formulas by Valela et al.¹⁶ and Wang et al.¹⁸, Eq. (23) incorporates an additional factor, ice cover roughness variation, thereby enhancing its comprehensiveness. Furthermore, it remains applicable across a wider range of effective parameters.

Conclusions and discussion

Variations in ice cover roughness alter the velocity distribution of flows beneath the ice cover, thereby influencing local scour processes around the pier. Therefore, accounting for the effects of ice cover roughness variations is more reasonable in the calculation of the maximum local scour depth around the pier under ice-covered flow conditions. The specific conclusions are as follows:

- (1) The presence of an ice cover modifies flow characteristics. As the ratio of ice cover roughness to bed roughness (n_i/n_b) increases, the maximum velocity point (U_{max}) shifts from $Z/H=0.68$ to $Z/H=0.35$, intensifying

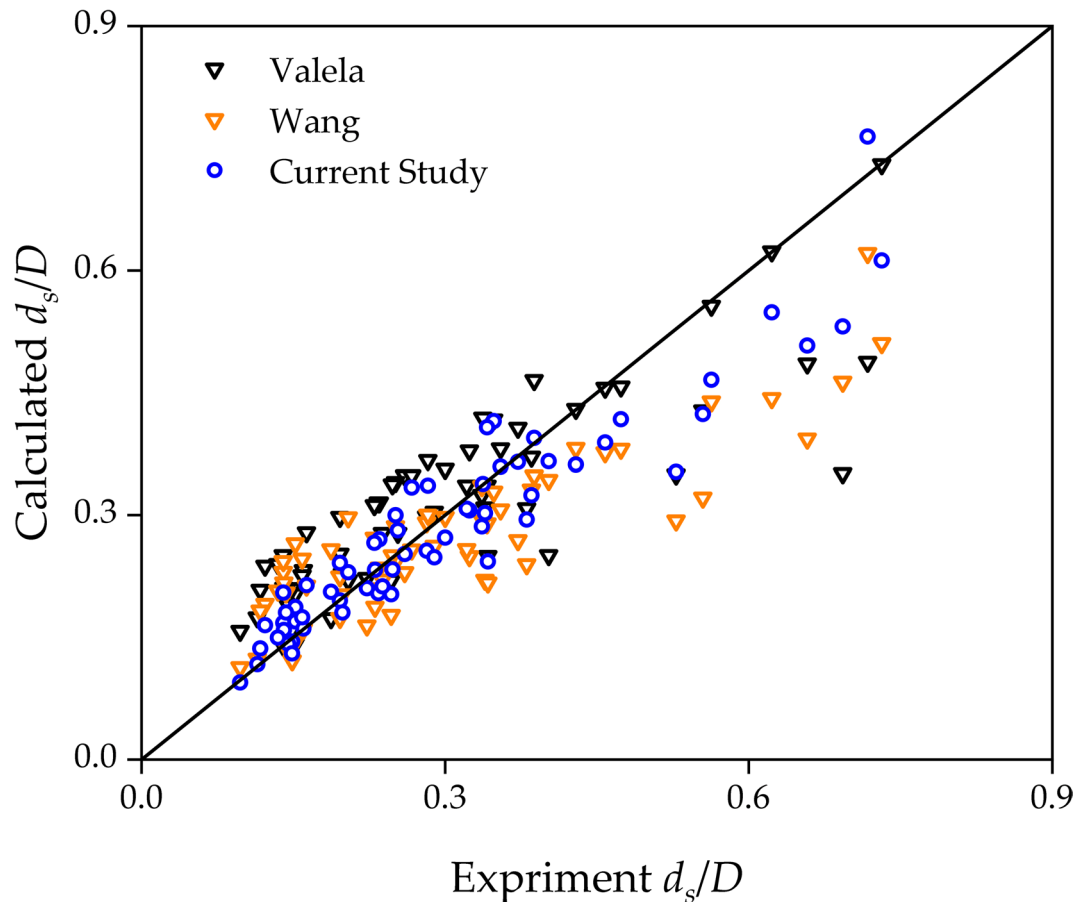


Fig. 18. Relationship between calculated and experimental scour depths around the pier under ice-covered flow conditions.

	MAPE	RMSE	MAE	R ²
Valela	26.61%	0.087	0.065	0.715
Wang	23.51%	0.092	0.068	0.768
Equation (23)	14.11%	0.059	0.042	0.883

Table 6. Error statistics of prediction equations for maximum local scour depth around the pier under ice-covered flow conditions.

the velocity gradient in the near-bed region and subsequently increasing bed shear stress by 7 to 42%. With increasing ice cover roughness, turbulent kinetic energy (TKE) near the riverbed increases by 8 to 35%. The combined effects of enhanced bed shear stress and TKE contribute to greater maximum local scour depths around the pier under rough ice-covered flow conditions.

- (2) Under identical conditions, the maximum local scour depth (d_s) increases with n_i/n_b . However, when $n_i/n_b < 1.9$, d_s shows a relatively rapid increase, whereas the rate of increase slows when $n_i/n_b > 1.9$. This is attributed to enhanced TKE generation beneath the ice cover increases energy dissipation in the flow, thereby reducing the amplification of near-bed TKE and bed shear stress, which subsequently attenuates the rate of increase in d_s .
- (3) Based on experimental data combined with numerical simulation results, a regression formula for calculating the maximum local scour depth around bridge piers under ice-covered flow conditions was derived by considering the n_i/n_b factor and its variations, along with specifying the applicable ranges of effective parameters. Compared with existing formulas in ice-covered pier scour literature, our proposed formula achieves the smallest calculation error by accounting for n_i/n_b variations and incorporating the broadest applicable ranges effective parameters.
- (4) Sensitivity analysis revealed that the flow Froude number exerts the most significant influence on scour depth prediction, serving as the most sensitive parameter. This is followed by the effects of n_i/n_b and d_{50}/D

ratios on pier scour under ice-covered flow conditions. Therefore, variations in ice cover roughness should be considered during bridge construction to accurately assess pier scour depth risks.

This study provides experimental data and a validated numerical model, focusing on investigating the impacts of ice cover roughness variations on flow characteristics and maximum local scour depth around bridge piers, thereby advancing research on pier scour processes under ice-covered flow conditions. The findings offer a tool for assessing scour risks to bridge infrastructure in cold regions. The numerical simulation method employed to calculate bridge pier scour depth is influenced by factors such as turbulence models and mesh resolution, leading to discrepancies between numerical and experimental results. Future work should focus on refining the model to improve accuracy. The experiment utilized non-uniform sediments, which undergo armor layer around the base of scour holes during pier scouring, thereby influencing the pier scour depth. The impact of sediment standard deviation variations on ice-induced pier scour requires further investigation. Future research also should further explore additional factors, such as varied pier shapes, arrangement patterns, and protective measures for bridge piers, to deepen the study and improve the accuracy of predicting maximum local scour depth around bridge piers under ice-covered flow conditions.

Data availability

The datasets used and/or analyzed during the current study are available from the corresponding author on request.

Received: 1 November 2025; Accepted: 28 December 2025

Published online: 14 January 2026

References

- Beltaos, S. Advances in river ice hydrology. *Hyd. Pro.* **14**(9), 1613–1625 (2000). [https://doi.org/10.1002/1099-1085\(20000630\)14:9%3C1613::AID-HYP73%3E3.0.CO;2-V](https://doi.org/10.1002/1099-1085(20000630)14:9%3C1613::AID-HYP73%3E3.0.CO;2-V)
- Luo, H. et al. An analytical study for predicting incipient motion velocity of sediments under ice cover. *Sci. Rep.* **15**(1), 1912. <https://doi.org/10.1038/s41598-025-85884-5> (2025).
- Jueyi, S. U. I., Jun, W. A. N. G., Yun, H. E. & Faye, K. R. O. L. Velocity profiles and incipient motion of frazil particles under ice cover. *Int. J. Sediment. Res.* **25**(1), 39–51. [https://doi.org/10.1016/S1001-6279\(10\)60026-1](https://doi.org/10.1016/S1001-6279(10)60026-1) (2010).
- Beltaos, S. Progress in the study and management of river ice jams. *Cold Reg. Sci. Technol.* **51**(1), 2–19. <https://doi.org/10.1016/j.coldregions.2007.09.001> (2008).
- Fan, G. et al. Study on scour simulation and boundary condition conversion technology for a shallow foundation bridge. *Sci. Rep.* **15**(1), 4581. <https://doi.org/10.1038/s41598-025-86549-z> (2025).
- Oliveto, G. & Hager, W. H. Temporal evolution of clear-water pier and abutment scour. *J. Hydraul. Eng.* **128**(9), 811–820. [https://doi.org/10.1061/\(ASCE\)0733-9429\(2002\)128:9\(811\)](https://doi.org/10.1061/(ASCE)0733-9429(2002)128:9(811)) (2002).
- Raudkivi, A. J. & Ettema, R. Clear-water scour at cylindrical piers. *J. Hydraul. Eng.* **109**(3), 338–350. [https://doi.org/10.1061/\(ASCE\)0733-9429\(1983\)109:3\(338\)](https://doi.org/10.1061/(ASCE)0733-9429(1983)109:3(338)) (1983).
- Dey, S., Bose, S. K. & Sastry, G. L. Clear water scour at circular piers: a model. *J. Hydrodyn.* **121**(12), 869–876. [https://doi.org/10.1061/\(ASCE\)0733-9429\(1995\)121:12\(869\)](https://doi.org/10.1061/(ASCE)0733-9429(1995)121:12(869)) (1995).
- Sato, H. Model experiments on hydraulic properties around multiple piers with reproduced 3D geometries. *Sci. Rep.* **12**(1), 19938. <https://doi.org/10.1038/s41598-022-24588-6> (2022).
- Ahmad, A. et al. Potential of roughening geometric elements as bridge pier local scour countermeasures. *Sci. Rep.* **15**, 8000. <https://doi.org/10.1038/s41598-025-92410-0> (2025).
- Zhao, S. et al. Suspended-sediment transport related to ice-cover conditions during cold and warm winters, Toudaoguai stretch of the Yellow River, Inner Mongolia, China. *Ecol. Indic.* **153**, 110435. <https://doi.org/10.1016/j.ecolind.2023.110435> (2023).
- Zabilansky, L. J. & White, K. D. Ice-cover effects on scour in narrow rivers. In *Proc. of the Third International Conference on Remediation of Contaminated Sediment* 11–14 (New Orleans, LA, USA, 2005).
- Wang, J., Sui, J. Y. & Karney, B. W. Incipient motion of non-cohesive sediment under ice cover—An experimental study. *J. Hydrodyn.* **20**(1), 117–124. [https://doi.org/10.1016/S1001-6058\(08\)60036-0](https://doi.org/10.1016/S1001-6058(08)60036-0) (2008).
- Wu, P., Hirshfield, F., Sui, J., Wang, J. & Chen, P. P. Impacts of ice cover on local scour around semi-circular bridge abutment. *J. Hydrodyn.* **26**(1), 10–18. [https://doi.org/10.1016/S1001-6058\(14\)60002-0](https://doi.org/10.1016/S1001-6058(14)60002-0) (2014).
- Wu, P., Balachandrar, R. & Sui, J. Local scour around bridge piers under ice-covered conditions. *J. Hydrodyn.* **142**(1), 04015038. [https://doi.org/10.1061/\(ASCE\)HY.1943-7900.0001063](https://doi.org/10.1061/(ASCE)HY.1943-7900.0001063) (2016).
- Valela, C., Sirianni, D. A., Nistor, I., Rennie, C. D. & Almansour, H. Bridge pier scour under ice cover. *Water* **13**(4), 536. <https://doi.org/10.3390/w13040536> (2021).
- Sirianni, D. A., Valela, C., Rennie, C. D., Nistor, I. & Almansour, H. Effects of developing ice covers on bridge pier scour. *J. Hydraul. Res.* **60**(4), 645–655. <https://doi.org/10.1080/00221686.2022.2041497> (2022).
- Wang, J., Wang, K., Fang, B. H. & Sui, J. A revisit of the local scour around bridge piers under an ice-covered flow condition—An experimental study. *J. Hydrodyn.* **33**(5), 928–937. <https://doi.org/10.1007/s42241-021-0082-0> (2021).
- Gao, P. et al. Study of flow characteristics and anti-scour protection around tandem piers under ice cover. *Buildings* **14**(11), 3478. <https://doi.org/10.3390/buildings14113478> (2024).
- Wang, C., Yu, X. & Liang, F. A review of bridge scour: mechanism, estimation, monitoring and countermeasures. *Nat. Hazards* **87**, 1881–1906. <https://doi.org/10.1007/s11069-017-2842-2> (2017).
- Qi, H. et al. Characteristics and mechanism of local scour reduction around spur dike using the collar in clear water. *Sci. Rep.* **14**(1), 12299. <https://doi.org/10.1038/s41598-024-63131-7> (2024).
- Richardson, J. E. & Panchang, V. G. Three-dimensional simulation of scour-inducing flow at bridge piers. *J. Hydraul. Eng.* **124**(5), 530–540. [https://doi.org/10.1061/\(ASCE\)0733-9429\(1998\)124:5\(530\)](https://doi.org/10.1061/(ASCE)0733-9429(1998)124:5(530)) (1998).
- Melville, B. W. & Raudkivi, A. J. Flow characteristics in local scour at bridge piers. *J. Hydraul. Eng.* **15**(4), 373–380. <https://doi.org/10.1080/00221687709499641> (1977).
- Khosronejad, A., Kang, S. & Sotiropoulos, F. Experimental and computational investigation of local scour around bridge piers. *Adv. Wat. Res.* **37**, 73–85. <https://doi.org/10.1016/j.advwatres.2011.09.013> (2012).
- Zhao, M., Cheng, L. & Zang, Z. Experimental and numerical investigation of local scour around a submerged vertical circular cylinder in steady currents. *Coa. Eng.* **57**(8), 709–721. <https://doi.org/10.1016/j.coastaleng.2010.03.002> (2010).
- Kalidindi, M. K. & Khosa, R. Evolution of coherent structures in the flow around a circular pier with a developing scour hole: A numerical study. *Phys. Fluids.* **36**(2), 025119. <https://doi.org/10.1063/5.0187905> (2024).

27. Hamidi, M., Sadeqlu, M. & Khalili, A. M. Investigating the design and arrangement of dual submerged vanes as mitigation countermeasure of bridge pier scour depth using a numerical approach. *Ocean Eng.* **299**, 117270. <https://doi.org/10.1016/j.oceaneng.2024.117270> (2024).
28. Al-Jubouri, M., Ray, R. P. & Abbas, E. H. Advanced numerical simulation of scour around bridge piers: Effects of pier geometry and debris on scour depth. *J. Mar. Sci. Eng.* **12**(9), 1637. <https://doi.org/10.3390/jmse12091637> (2024).
29. Hamidi, M., Koohsari, A. & Khalili, A. M. Numerical investigation of mining pit effects on maximum scour depth around bridge pier with different shape. *Model. Earth Syst. Environ.* **10**, 5189–5203. <https://doi.org/10.1007/s40808-024-02057-5> (2024).
30. Gupta, L. K., Pandey, M. & Raj, P. A. Numerical simulation of local scour around the pier with and without airfoil collar (AFC) using FLOW-3D. *Environ. Fluid. Mech.* **24**, 631–649. <https://doi.org/10.1007/s10652-023-09932-2> (2024).
31. Cheng, T. et al. The impact of ice on river morphology and hydraulic structures: A review. *Water* **17**(4), 480. <https://doi.org/10.3390/w17040480> (2025).
32. Namaee, M. R., Wu, P. & Dziedzic, M. Numerical modeling of local scour in the vicinity of bridge abutments when covered with ice. *Water* **15**(19), 3330. <https://doi.org/10.3390/w15193330> (2023).
33. Namaee, M. R., Sui, J., Wu, Y. & Linklater, N. Three-dimensional numerical simulation of local scour around circular side-by-side bridge piers with ice cover. *Can. J. Civil. Eng.* **48**(10), 1335–1353. <https://doi.org/10.1139/cjce-2019-0360> (2021).
34. Gao, P. et al. Refined simulation study of hydrodynamic properties and flow field characteristics around tandem bridge piers under ice-cover conditions. *Buildings* **14**(9), 2853. <https://doi.org/10.3390/buildings14092853> (2024).
35. Melville, B. W. & Sutherland, A. J. Design method for local scour at bridge piers. *J. Hydraul. Eng. ASCE* **114**, 1210–1226. [https://doi.org/10.1061/\(asce\)0733-9429\(1988\)114:10\(1210\)](https://doi.org/10.1061/(asce)0733-9429(1988)114:10(1210)) (1988).
36. Lança, R. M., Fael, C. S., Maia, R. J., Pêgo, J. P. & Cardoso, A. H. Clear-water scour at comparatively large cylindrical piers. *J. Hydraul. Eng.* **139**(11), 1117–1125. [https://doi.org/10.1061/\(ASCE\)HY.1943-7900.0000788](https://doi.org/10.1061/(ASCE)HY.1943-7900.0000788) (2013).
37. Dong, S. et al. Analysis of local scour around double piers in tandem arrangement in an S-shaped channel under ice-jammed flow conditions. *Water* **16**(19), 2831. <https://doi.org/10.3390/w16192831> (2024).
38. Li, G., Sui, J. & Sediqi, S. Hydrodynamic characteristics in pools with leafless vegetation under ice-covered flow conditions—An experimental study and numerical simulation. *J. Hydrol.* **657**, 133135. <https://doi.org/10.1016/j.jhydrol.2025.133135> (2025).
39. Li, G., Sui, J. & Dziedzic, M. Local scour and hydrodynamics around river crossing pipelines under ice-covered flow conditions. *Ocean Eng.* **336**, 121835. <https://doi.org/10.1016/j.oceaneng.2025.121835> (2025).
40. Sediqi, S., Sui, J. & Li, G. Local scour around Bridge abutments in vegetated beds under ice-covered flow conditions—An experimental study and mathematical assessment using machine learning methods. *J. Hydrol.* **659**, 133257. <https://doi.org/10.1016/j.jhydrol.2025.133257> (2025).
41. Li, S. S. Estimates of the Manning's coefficient for ice-covered rivers. In *Proceedings of the Institution of Civil Engineers-Water Management*, **165**(9), 455–505 (Thomas Telford Ltd, 2012) <https://doi.org/10.1680/wama.11.00017>.
42. Barahimi, M. & Sui, J. Deformation of vegetated channel bed under ice-covered flow conditions. *J. Hydrol.* **636**, 131280. <https://doi.org/10.1016/j.jhydrol.2024.131280> (2024).
43. Carey, K. L. Observed Configuration and Computed Roughness of the Underside of River Ice, St. Croix River, Wisconsin. US Geological Survey Professional Paper, 550. (1966).
44. Hager, W. H. *Wastewater Hydraulics: Theory and Practice* (Springer Science & Business Media, 2010).
45. Mia, F. & Nago, H. Design method of time-dependent local scour at circular bridge pier. *J. Hydraul. Eng. ASCE* **129**, 420–427. [https://doi.org/10.1061/\(asce\)0733-9429\(2003\)129:6\(420\)](https://doi.org/10.1061/(asce)0733-9429(2003)129:6(420)) (2003).
46. Hirt, C. W. & Nichols, B. D. Volume of fluid (VOF) method for the dynamics of free boundaries. *J. Com. Phy.* **39**(1), 201–225. [https://doi.org/10.1016/0021-9991\(81\)90145-5](https://doi.org/10.1016/0021-9991(81)90145-5) (1981).
47. *FLOW-3D User's Manual Version 11.1*
48. Hirt, C. W. & Sicilian, J. M. A porosity technique for the definition of obstacles in rectangular cell meshes. In *International Conference on Numerical Ship Hydrodynamics, 4th* (1985).
49. Nielsen, A. W., Liu, X., Sumer, B. M. & Fredsøe, J. Flow and bed shear stresses in scour protections around a pile in a current. *Coastal Eng.* **72**, 20–38. <https://doi.org/10.1016/j.coastaleng.2012.09.001> (2013).
50. Li, G., Sui, J., Dziedzic, M. & Ali, F. Local scour around submerged spur dikes under ice-covered conditions: Experimental and numerical investigation. *Cold Reg. Sci. Tech.* **241**, 104695. <https://doi.org/10.1016/j.coldregions.2025.104695> (2026).
51. Yakhot, V. & Smith, L. M. The renormalization group, the ϵ -expansion and derivation of turbulence models. *J. Sci. Com.* **7**(1), 35–61. <https://doi.org/10.1007/BF01060210> (1992).
52. Yakhot, V., Orszag, S. A., Thangam, S., Gatski, T. B. & Speziale, C. G. Development of turbulence models for shear flows by a double expansion technique. *Phys. Fluids A* **4**(7), 1510–1520. <https://doi.org/10.1063/1.858424> (1992).
53. Soulsby, R. L. & Whitehouse, R. J. S. Threshold of sediment motion in coastal environments. In *Pacific Coasts and Ports' 97: Proceedings of the 13th Australasian Coastal and Ocean Engineering Conference and the 6th Australasian Port and Harbour Conference*. Vol. 1, 145–150. (Centre for Advanced Engineering, University of Canterbury, Christchurch, New Zealand, 1997).
54. Mastbergen, D. R. & Van Den Berg, J. H. Breaching in fine sands and the generation of sustained turbidity currents in submarine canyons. *Sedimentology* **50**(4), 625–637. <https://doi.org/10.1046/j.1365-3091.2003.00554.x> (2003).
55. Soulsby, R. *Dynamics of Marine Sands: A Manual for Practical Applications* (Thomas Telford, London, 1997).
56. Meyer-Peter, E. & Muller, R. *Formulas for Bed-Load Transport*. IAHR 2nd meeting, Stockholm, appendix 2. (IAHR, 1948).
57. Li, A. B., Zhang, G. G., Chandara, M. & Zhou, S. Influence of sediment transport rate formula on numerical simulation of local scour around a bridge pier. *J. Sed. Res.* **47**, 15–22 (2022).
58. Sarker, M. A. Flow measurement around scoured bridge piers using acoustic-doppler velocimeter (ADV). *Flow. Mea. Ins.* **9**(4), 217–227. [https://doi.org/10.1016/S0955-5986\(98\)00028-4](https://doi.org/10.1016/S0955-5986(98)00028-4) (1998).
59. Celik, I. B., Ghia, U., Roache, P. J. & Freitas, C. J. Procedure for estimation and reporting of uncertainty due to discretization in CFD applications. *J. Fluids. Eng. Trans. ASME* **130**(7), 078001. <https://doi.org/10.1115/1.2960953> (2008).
60. Vaghefi, M., Ghodsian, M. & Salimi, S. Scour formation due to laterally inclined circular pier. *Arabian J. Sci. Eng.* **41**(4), 1311–1318. <https://doi.org/10.1007/s13369-015-1920-6> (2016).
61. Shen, H. T. & Harden, T. O. The effect of ice cover on vertical transfer in stream channels 1. *JAWRA J. Am. Water Resour. Assoc.* **14**(6), 1429–1439. <https://doi.org/10.1111/j.1752-1688.1978.tb02293.x> (1978).
62. Kim, H. S., Nabi, M., Kimura, I. & Shimizu, Y. Numerical investigation of local scour at two adjacent cylinders. *Adv. Wat. Res.* **70**, 131–147. <https://doi.org/10.1016/j.advwatres.2014.04.018> (2014).
63. Yoon, J. Y., Patel, V. C. & Ettema, R. Numerical model of flow in ice-covered channel. *J. Hydraul. Eng.* **122**(1), 19–26. [https://doi.org/10.1061/\(ASCE\)0733-9429\(1996\)122:1\(19\)](https://doi.org/10.1061/(ASCE)0733-9429(1996)122:1(19)) (1996).
64. Nakagawa, H. *Turbulence in Open Channel Flows*. (Routledge, 2017).

Acknowledgements

The authors are grateful for the Joint Funds of the National Natural Science Foundation of China.

Author contributions

S.D.: laboratory works, data curation, formal analysis, methodology, and writing—original draft preparation;

Z.Z.: conceptualization, laboratory supervision, and methodology; J.S.: conceptualization, methodology, and writing—review and editing; J.W.: conceptualization, laboratory supervision, methodology, and writing—review and editing.

Funding

This study was supported by the Joint Funds of the National Natural Science Foundation of China (NSFC) under grant numbers U2443221 and U2243239.

Declarations

Competing interests

The authors declare no competing interests.

Additional information

Correspondence and requests for materials should be addressed to J.W.

Reprints and permissions information is available at www.nature.com/reprints.

Publisher's note Springer Nature remains neutral with regard to jurisdictional claims in published maps and institutional affiliations.

Open Access This article is licensed under a Creative Commons Attribution-NonCommercial-NoDerivatives 4.0 International License, which permits any non-commercial use, sharing, distribution and reproduction in any medium or format, as long as you give appropriate credit to the original author(s) and the source, provide a link to the Creative Commons licence, and indicate if you modified the licensed material. You do not have permission under this licence to share adapted material derived from this article or parts of it. The images or other third party material in this article are included in the article's Creative Commons licence, unless indicated otherwise in a credit line to the material. If material is not included in the article's Creative Commons licence and your intended use is not permitted by statutory regulation or exceeds the permitted use, you will need to obtain permission directly from the copyright holder. To view a copy of this licence, visit <http://creativecommons.org/licenses/by-nc-nd/4.0/>.

© The Author(s) 2026